

PAPER • OPEN ACCESS

Algebraic expressions for the polarisation response of spin-VCSELs


To cite this article: Mike Adams *et al* 2018 *Semicond. Sci. Technol.* **33** 064002

View the [article online](#) for updates and enhancements.

Related content

- [Spin-polarized properties of optically pumped VCSELs](#)
A Dyson and M J Adams
- [Polarization and transverse-mode selection in quantum-well vertical-cavity surface-emitting lasers: index- and gain-guided devices](#)
J Martín-Regalado, S Balle, M San Miguel et al.
- [Non-degenerate ROs of VCSELs](#)
D L Boiko, E Le Cren, G M Stéphan et al.

Algebraic expressions for the polarisation response of spin-VCSELs

Mike Adams¹ , Nianqiang Li¹, Ben Cemlyn¹, Hadi Susanto² and Ian Henning¹

¹ School of Computer Engineering and Electronics Engineering, University of Essex, Wivenhoe Park, Colchester CO4 3SQ, United Kingdom

² Department of Mathematical Sciences, University of Essex, Wivenhoe Park, Colchester CO4 3SQ, United Kingdom

E-mail: adammm@essex.ac.uk

Received 6 February 2018, revised 23 March 2018

Accepted for publication 12 April 2018

Published 2 May 2018



Abstract

Closed-form expressions are derived for the relationship between the polarisation of the output and that of the pump for spin-polarised vertical-cavity surface-emitting lasers. These expressions are based on the spin-flip model (SFM) combined with the condition that the carrier recombination time is much greater than both the spin relaxation time and the photon lifetime. Allowance is also included for misalignment between the principal axes of birefringence and dichroism. These expressions yield results that are in excellent agreement both with previously published numerical calculations and with further tests for a wide range of parameters. Trends with key parameters of the SFM are easily deduced from these expressions.

Keywords: vertical-cavity surface-emitting lasers, spin injection, spin-flip model

(Some figures may appear in colour only in the online journal)

1. Introduction

Research on spin-polarised vertical-cavity surface-emitting lasers (spin-VCSELs) is a relatively new direction within optoelectronics. The manipulation of the unique quantum mechanical property of spin has been treated traditionally as a fundamental challenge of physics. Topics such as magnetoresistance, spin-dependent transport, spin coherence length, synthesis of spintronic materials and quantum computation are receiving significant attention [1]. Demonstrations of spin-polarised LEDs and lasers [2], although less well-known, represent the first ground-breaking steps in spin optoelectronics. These spin-controlled light sources have important potential applications in optical information processing and data storage, optical communication, quantum computing and bio-chemical sensing.

Spin-VCSELs can offer threshold reduction [3–6], polarisation control [7–11] and high-speed dynamics [11–17]. Experimental work on these topics has been supported by theoretical analyses using various models. Since the operation principle of spin-VCSELs depends upon injection of spin-polarised electrons which then recombine preferentially with emission of polarised light, the simplest model uses rate equations for the spin-up and spin-down carrier concentrations (n^+ and n^- , respectively) and right- and left-circularly polarised (RCP, LCP) photon densities [18–21]. In addition to the usual terms for carrier recombination rate γ and photon field decay rate κ , interaction of the spin-polarised electrons is accounted for by a spin relaxation rate γ_j . For quantum well (QW) active regions, rate equations can be included for carriers in the wells and in the barriers [3, 4, 22] with a carrier capture rate used to couple the two sets of populations. For quantum dot (QD) active regions the equations for the barriers are replaced by corresponding ones for the wetting layers [23, 24]. Other refinements, such as including the effects of gain saturation, spin-polarised hole concentrations, spontaneous emission into the mode, etc, have also been implemented in the rate equation model.



Original content from this work may be used under the terms of the [Creative Commons Attribution 3.0 licence](https://creativecommons.org/licenses/by/3.0/). Any further distribution of this work must maintain attribution to the author(s) and the title of the work, journal citation and DOI.

The spin-flip model (SFM) [25–27] offers a more detailed description of polarisation dynamics in spin lasers by including RCP and LCP field amplitudes and phases, non-linear dispersion via the linewidth enhancement factor α , and field interactions arising from nonlinear anisotropies, i.e. birefringence, γ_p , and dichroism, γ_a . These interactions provided the basis for explanations of polarisation switching (PS) between orthogonal linearly polarised (LP) modes in conventional VCSELs [26, 28]. In spin-VCSELs the SFM rate equations include the polarisation of the optical pump [27] so that it can be used to describe PS for circularly-polarised pumping [29] and, more generally, the response of the output polarisation to variation of the pump polarisation from RCP through LP to LCP [10, 11, 30, 31]. In addition the SFM has been used [11–14, 16, 17] to explain experimental results on high-speed polarisation oscillations. These are the result of competition between the spin-flip processes that tend to equalise the gain for the RCP and LCP fields, the dichroism which tries to equalise the field amplitudes and the birefringence which couples power between the polarised fields [27].

An ‘extended SFM’ includes a realistic spectral dependence of the gain and the index of refraction of QWs [32]; in this model γ_a is a pure loss anisotropy whilst the differences in material gain due to the frequency splitting between the modes are included in the gain model. Further developments of the SFM take account of misalignment between the principal axes of the birefringence and dichroism [33], descriptions of the spatial variation of the electromagnetic modes and the carrier densities [34], inclusion of thermal effects [35], and extension to QD active regions in spin-VCSELs [36, 37]. This increasing sophistication of treatment comes at a price: the numerical computation required to solve the equations for wide ranges of, frequently unknown, parameter values means that it is often difficult to see trends and thus obtain guidance to support further experimental studies. Even the basic SFM rate equations in steady-state have to be solved numerically as there is no algebraic solution to the best of our knowledge. Hence the present contribution addresses the problem of finding accessible algebraic expressions for the polarisation response (output ellipticity versus pump ellipticity) and hence to determine trends with parameters. No attempt will be made here to model frequency dependence of the refractive index and gain, spatial variation of the electromagnetic modes and the carrier densities, thermal effects or any other details. Attention is restricted to the basic SFM equations.

For conventional VCSELs, Erneux *et al* [38] have developed a two-variable reduction of the SFM equations that leads to algebraic relations for the linearly-polarised and elliptically-polarised steady-state solutions. In order to do this, they considered the commonly-encountered situation that the carrier recombination time was much greater than both the spin relaxation time and the photon lifetime, i.e. in terms of the SFM rates, $\gamma \ll \gamma_s$ and $\gamma \ll \kappa$. Here it should be noted that the ‘effective’ spin relaxation rate γ_s in the SFM is related to the spin relaxation rate γ_j measured experimentally by the equation $\gamma_s = 2\gamma_j + \gamma$ [25]. The objective here is to extend the treatment of [38] to include polarised pumping, as

in spin-VCSELs. In addition, in the interest of generality, allowance for misalignment of the birefringence and dichroism will be made, since this has been shown to be important for interpreting chaotic and bistable polarisation dynamics in VCSELs [39, 40].

2. Theory

The SFM equations can be expressed in terms of the RCP and LCP field amplitudes, R_+ , R_- , and phase difference ϕ by using the amplitude/phase decomposition of the fields $E_{\pm} = R_{\pm} \exp(i\psi_{\pm})$ and defining $\phi = \psi_+ - \psi_-$. Allowing for polarised pumping with ellipticity P , the equations become

$$\frac{dR_+}{dt} = \kappa(N + m - 1)R_+ - (\bar{\gamma}_a \cos \phi + \bar{\gamma}_p^+ \sin \phi)R_-, \quad (1)$$

$$\frac{dR_-}{dt} = \kappa(N - m - 1)R_- - (\bar{\gamma}_a \cos \phi - \bar{\gamma}_p^- \sin \phi)R_+, \quad (2)$$

$$\begin{aligned} \frac{d\phi}{dt} = 2\kappa\alpha m + \left(\bar{\gamma}_p^- \frac{R_+}{R_-} - \bar{\gamma}_p^+ \frac{R_-}{R_+} \right) \cos \phi \\ + \left(\frac{R_+}{R_-} + \frac{R_-}{R_+} \right) \bar{\gamma}_a \sin \phi, \end{aligned} \quad (3)$$

$$\frac{dN}{dt} = \gamma[\eta - (1 + R_+^2 + R_-^2)N - (R_+^2 - R_-^2)m], \quad (4)$$

$$\frac{dm}{dt} = \gamma P\eta - [\gamma_s + \gamma(R_+^2 + R_-^2)]m - \gamma(R_+^2 - R_-^2)N, \quad (5)$$

where

$$\begin{aligned} \bar{\gamma}_p^+ &= \gamma_p - \gamma_a \sin(2\theta), \quad \bar{\gamma}_p^- = \gamma_p + \gamma_a \sin(2\theta), \\ \bar{\gamma}_a &= \gamma_a \cos(2\theta), \end{aligned}$$

with θ defined as the angle between the axis of maximum frequency and the axis of maximum losses [33]. The normalised carrier variables N and m here are proportional to the sum ($n^+ + n^-$) and difference ($n^+ - n^-$), respectively, of the spin-up/down carrier concentrations. The normalised pumping rate, denoted by η , is the sum of the RCP and LCP normalised pumping rates, and the other parameters appearing in (1)–(5) have already been defined above.

Following the approach in [38] but allowing for non-zero P , the approximate steady-state versions of equations (4) and (5), respectively, yield

$$R_+^2 + R_-^2 = \eta - 1, \quad (6)$$

$$m = \frac{\gamma}{\gamma_s} [P\eta - \varepsilon(\eta - 1)], \quad (7)$$

where the ellipticity ε of the VCSEL output is defined [27] as

$$\varepsilon = \frac{R_+^2 - R_-^2}{R_+^2 + R_-^2}. \quad (8)$$

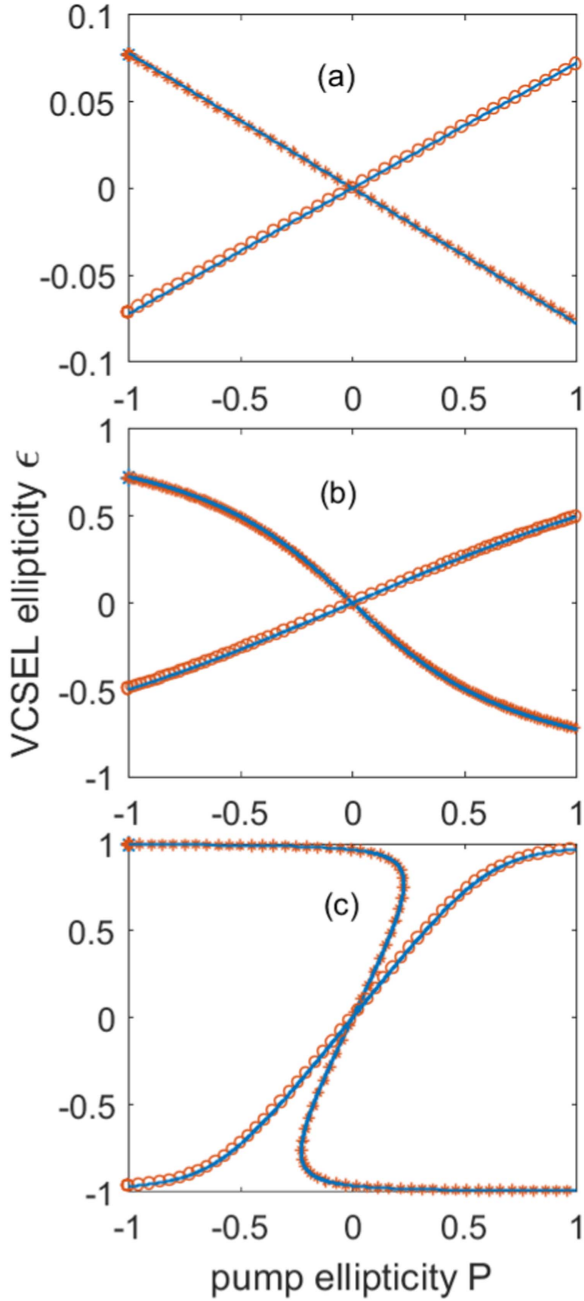


Figure 1. VCSEL ellipticity versus pump ellipticity for parameter values $\gamma_s = 100 \text{ ns}^{-1}$, $\gamma = 1 \text{ ns}^{-1}$, $\kappa = 125 \text{ ns}^{-1}$, $\alpha = 3$, $\eta = 2$, $\gamma_a = 0.2 \text{ ns}^{-1}$, with (a) $\gamma_p = 100 \text{ ns}^{-1}$, (b) $\gamma_p = 10 \text{ ns}^{-1}$, (c) $\gamma_p = 1 \text{ ns}^{-1}$. Solid lines: results from equation (18). Circles: numerical results for out-of-phase solution. Asterisks: numerical results for in-phase solution.

Equation (6) is an energy conservation relation, whilst equation (7) allows the variable m to be eliminated from the remaining equations.

From (6) and (8) it follows that

$$R_+ = \sqrt{\frac{(1 + \varepsilon)(\eta - 1)}{2}}, \quad R_- = \sqrt{\frac{(1 - \varepsilon)(\eta - 1)}{2}}. \quad (9)$$

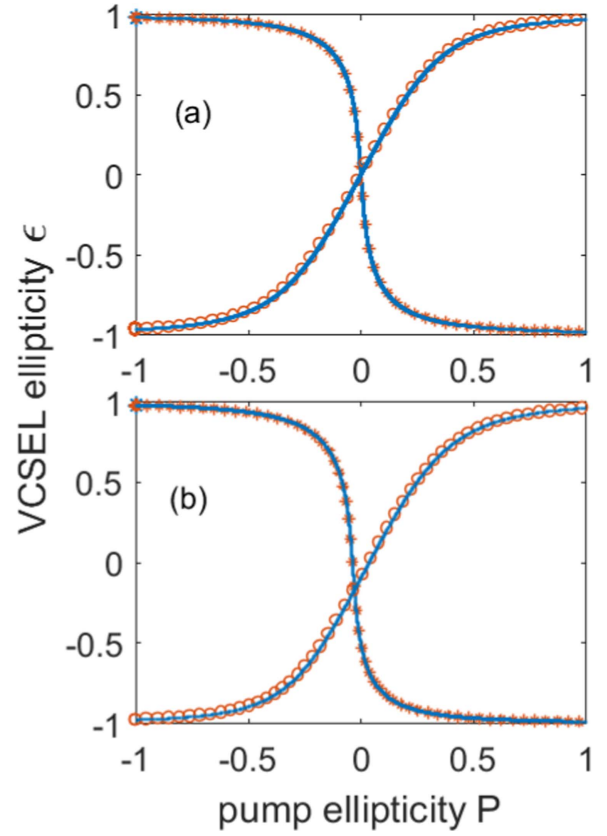


Figure 2. VCSEL ellipticity versus pump ellipticity for parameter values $\gamma_s = 100 \text{ ns}^{-1}$, $\gamma = 1 \text{ ns}^{-1}$, $\kappa = 125 \text{ ns}^{-1}$, $\alpha = 3$, $\eta = 1.2$, $\gamma_a = 0.2 \text{ ns}^{-1}$, $\gamma_p = 1 \text{ ns}^{-1}$, with (a) $\theta = 0^\circ$ (b) $\theta = 30^\circ$. Solid lines: results from equation (17). Circles: numerical results for out-of-phase solution. Asterisks: numerical results for in-phase solution.

Multiplying the steady-state versions of equations (1) and (2) by R_+ and R_- , respectively, and subtracting yields

$$\kappa(N - 1)(R_+^2 - R_-^2) + \kappa m(R_+^2 + R_-^2) = 2R_+R_- \times (\bar{\gamma}_p^+ + \bar{\gamma}_p^-) \sin \varphi. \quad (10)$$

Substituting the results of (7) and (9) in (10) then gives an expression for $(N - 1)$:

$$N - 1 = -\frac{\gamma}{\gamma_s} \frac{1}{\varepsilon} [P\eta - \varepsilon(\eta - 1)] + \frac{\sqrt{1 - \varepsilon^2}}{\varepsilon} \times \frac{(\bar{\gamma}_p^+ + \bar{\gamma}_p^-)}{2\kappa} \sin \phi. \quad (11)$$

Hence, using (7), (9) and (11), equation (1) can be expressed as

$$\frac{\gamma}{\gamma_s} \frac{(\varepsilon - 1)}{\varepsilon} [P\eta - \varepsilon(\eta - 1)] + \frac{\gamma_p}{\kappa} \frac{\sqrt{1 - \varepsilon^2}}{\varepsilon} \times \frac{(\bar{\gamma}_p^+ + \bar{\gamma}_p^-)}{2\kappa} \sin \phi = \left(\frac{\bar{\gamma}_a}{\kappa} \cos \phi + \frac{\bar{\gamma}_p^+}{\kappa} \sin \phi \right) \sqrt{\frac{1 - \varepsilon}{1 + \varepsilon}}, \quad (12)$$

which simplifies to

$$\frac{\gamma}{\gamma_s}[P\eta - \varepsilon(\eta - 1)]\sqrt{1 - \varepsilon^2} = -\varepsilon\frac{\bar{\gamma}_a}{\kappa}\cos\phi + \frac{[(1 - \varepsilon)\bar{\gamma}_p^+ + (1 + \varepsilon)\bar{\gamma}_p^-]}{2\kappa}\sin\phi. \quad (13)$$

Similarly, using (7) and (9), in the steady state equation (3) can be written in the form

$$\alpha\frac{\gamma}{\gamma_s}[P\eta - \varepsilon(\eta - 1)]\sqrt{1 - \varepsilon^2} = -\frac{\bar{\gamma}_a}{\kappa}\sin\phi + \frac{[(1 - \varepsilon)\bar{\gamma}_p^+ - (1 + \varepsilon)\bar{\gamma}_p^-]}{2\kappa}\cos\phi. \quad (14)$$

Equations (13) and (14) are implicit relations for the phase difference ϕ in terms of the normalised pumping rate η , the ellipticity of the pump P and the ellipticity of the output ε . These equations can be rewritten to give the following expressions for $\sin\phi$ and $\cos\phi$:

$$\sin\phi = -\frac{\gamma}{\gamma_s}[P\eta - \varepsilon(\eta - 1)]\sqrt{1 - \varepsilon^2} \times \frac{2\kappa\{2\alpha\varepsilon\bar{\gamma}_a + [(1 - \varepsilon)\bar{\gamma}_p^+ - (1 + \varepsilon)\bar{\gamma}_p^-]\}}{4\varepsilon\bar{\gamma}_a^2 - [(1 - \varepsilon)^2\bar{\gamma}_p^{+2} - (1 + \varepsilon)^2\bar{\gamma}_p^{-2}]}, \quad (15)$$

$$\cos\phi = -\frac{\gamma}{\gamma_s}[P\eta - \varepsilon(\eta - 1)]\sqrt{1 - \varepsilon^2} \times \frac{2\kappa\{2\bar{\gamma}_a + \alpha[(1 - \varepsilon)\bar{\gamma}_p^+ + (1 + \varepsilon)\bar{\gamma}_p^-]\}}{4\varepsilon\bar{\gamma}_a^2 - [(1 - \varepsilon)^2\bar{\gamma}_p^{+2} - (1 + \varepsilon)^2\bar{\gamma}_p^{-2}]}. \quad (16)$$

Eliminating ϕ from (15) and (16) gives

$$P = \varepsilon\left(\frac{\eta - 1}{\eta}\right) \pm \frac{\gamma_s}{2\eta\gamma\kappa\sqrt{1 - \varepsilon^2}} \times \frac{4\varepsilon\bar{\gamma}_a^2 - [(1 - \varepsilon)^2\bar{\gamma}_p^{+2} - (1 + \varepsilon)^2\bar{\gamma}_p^{-2}]}{\sqrt{\{2\alpha\varepsilon\bar{\gamma}_a + [(1 - \varepsilon)\bar{\gamma}_p^+ - (1 + \varepsilon)\bar{\gamma}_p^-]\}^2 + \{2\bar{\gamma}_a + \alpha[(1 - \varepsilon)\bar{\gamma}_p^+ + (1 + \varepsilon)\bar{\gamma}_p^-]\}^2}}. \quad (17)$$

Equation (17) is an implicit relation between the normalised pumping rate η , the ellipticity of the pump P and the ellipticity of the output ε . The sign of the square root term leads to the selection of in-phase or out-of-phase solutions; these correspond, respectively, to cases where the phase difference ϕ is the ‘continuation’ of 0 or π , for the LP solutions. The stability of the general elliptically-polarised solutions has been studied recently by a combination of numerical, asymptotic and bifurcation analyses of the SFM rate equations (for the case where there is no misalignment of birefringence and dichroism) [41, 42].

For the case $\theta = 0$, i.e. no misalignment of birefringence and dichroism, equation (17) reduces to

$$P = \frac{\varepsilon}{\eta}\left[\eta - 1 \pm \frac{\gamma_s(\gamma_a^2 + \gamma_p^2)}{\gamma\kappa\sqrt{1 - \varepsilon^2}}\right] \times \frac{1}{\sqrt{(\gamma_a + \alpha\gamma_p)^2 + \varepsilon^2(\alpha\gamma_a - \gamma_p)^2}}. \quad (18)$$

For the case of $P = 0$ equation (18) reduces to equation (59) of [38] where it describes elliptically-polarised solutions of the SFM for unpolarised pumping. In the general case, it can be used to generate plots of ε versus P for given values of η and various combinations of parameters provided that $\gamma \ll \gamma_s$, $\gamma \ll \kappa$.

For small values of ε , equation (18) can be simplified to the form:

$$\varepsilon \approx \frac{P\eta}{\eta - 1 \pm \frac{\gamma_s(\gamma_a^2 + \gamma_p^2)}{\gamma\kappa(\gamma_a + \alpha\gamma_p)}}. \quad (19)$$

This approximate result can be used to easily estimate the effect of the SFM parameters on the rate of change of output ellipticity with pump ellipticity for relatively weak ellipticity.

3. Numerical examples

Equations (17)–(19) are the main results of this contribution. We have verified that the approximation of equation (18) gives excellent agreement with plots of P versus ε that were calculated numerically in previous publications from our group [10, 11, 17, 31, 41]. In particular the trends with γ_s/γ , γ_p/κ , α and η that were revealed in [31] for the case of $\gamma_a = 0$ are maintained in the present approximation also for non-zero

dichroism. Further tests of the algebraic expressions against numerical solutions of the steady-state SFM equations will now be presented.

Figure 1 compares numerical solutions of the steady-state SFM equations with results from equation (18) for the case when there is no misalignment of birefringence and dichroism. The values of parameters used are $\gamma_s = 100 \text{ ns}^{-1}$, $\gamma = 1 \text{ ns}^{-1}$, $\kappa = 125 \text{ ns}^{-1}$, $\alpha = 3$, $\eta = 2$, $\gamma_a = 0.2 \text{ ns}^{-1}$, with (a) $\gamma_p = 100 \text{ ns}^{-1}$, (b) $\gamma_p = 10 \text{ ns}^{-1}$, (c) $\gamma_p = 1 \text{ ns}^{-1}$. Out-of-phase and in-phase solutions are distinguished by the use of circles and asterisks, respectively,

for the numerical results. Clearly there is excellent agreement between the numerical and analytical results. It is also worth noting that the restriction that γ_p be of the same order as γ that was required for accuracy of the approximation in [38] is not needed here. The strong effect of birefringence rate γ_p on the polarisation response is well illustrated in figure 1 (note the different scales on the vertical axes of (a)–(c)).

The in-phase solution in figure 1(c) shows a ‘Z’-shaped response which is different from those in figures 1(a) and (b). The relationship between SFM parameters that gives this behaviour can be found by requiring that the RHS of equation (18) is zero at $\varepsilon = 0$ for the in-phase solution. The result is

$$\eta_b - 1 = \frac{\gamma_s(\gamma_a^2 + \gamma_p^2)}{\gamma\kappa(\gamma_a + \alpha\gamma_p)}, \quad (20)$$

where η_b is the minimum normalised pump rate that allows the polarisation response to change from positive to negative slope for the values of parameters appearing on the RHS of (20). For the parameter values used in figure 1(c) equation (20) gives $\eta_b = 1.26$. Figure 2(a) shows results for the same parameter values as in figure 1(c) but here the normalised pump rate is 1.2, and hence there is no change in the sign of the slope of the calculated response for the in-phase solution.

Figure 2(b) shows results for misalignment of birefringence and dichroism by an angle of 30° . Again there is excellent agreement between numerical and analytical results from equation (17) in figure 2. It is observed that for the misaligned case the in-phase and out-of-phase solutions cross at non-zero values of P and ε . The co-ordinates $(\varepsilon_{cp}, P_{cp})$ of the crossing point can be calculated from the condition that the last term on the RHS of equation (17) is zero. This condition yields

$$\varepsilon_{cp} = \frac{-(\gamma_a^2 + \gamma_p^2) + \sqrt{(\gamma_a^2 + \gamma_p^2)^2 - 4\gamma_a^2\gamma_p^2 \sin^2(2\theta)}}{2\gamma_a\gamma_p \sin(2\theta)}, \quad (21)$$

$$P_{cp} = \varepsilon_{cp} \left(\frac{\eta - 1}{\eta} \right). \quad (22)$$

Equations (21) and (22) are found to give excellent agreement with the calculated crossing point of the solutions in figure 2(b) at $(-0.0286, -0.1714)$, and it is worth noting that they are independent of the parameters γ_s , γ , κ and α .

Figure 3 shows another comparison of aligned and misaligned axes of birefringence and dichroism. In this case the parameter values are $\gamma_s = 100 \text{ ns}^{-1}$, $\gamma = 1 \text{ ns}^{-1}$, $\kappa = 125 \text{ ns}^{-1}$, $\alpha = 3$, $\eta = 1.2$, $\gamma_a = 0.1 \text{ ns}^{-1}$, $\gamma_p = 0.1 \text{ ns}^{-1}$, with (a) $\theta = 0^\circ$ (b) $\theta = 20^\circ$. Once again the results of equation (17) pass this test with flying colours. Again the crossing point co-ordinates $(-0.0607, -0.364)$ from equations (21) and (22) are in agreement with those found in figure 3(b).

It should be noted that, although numerical results have been presented for both in-phase and out-of-phase solutions, no attempt has been made here at a stability analysis of these solutions. In many cases only one solution will be stable so

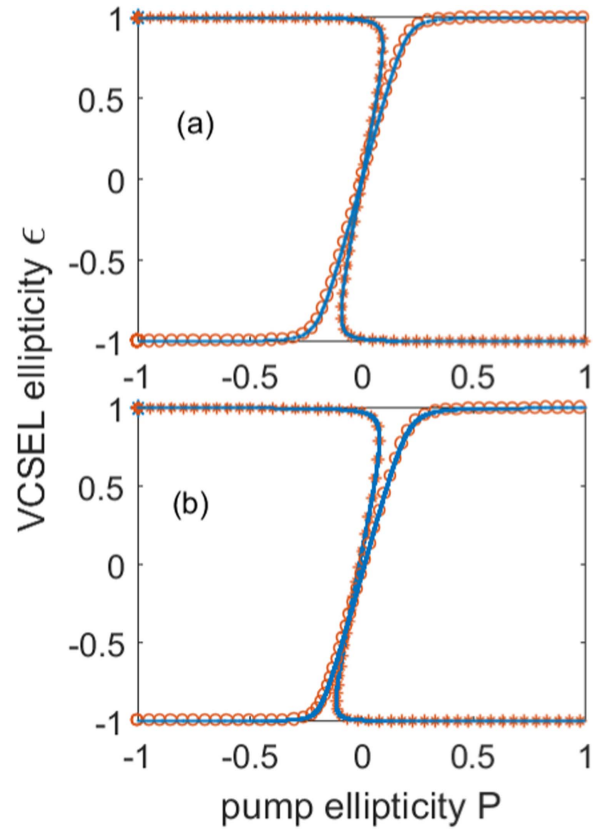


Figure 3. VCSEL ellipticity versus pump ellipticity for parameter values $\gamma_s = 100 \text{ ns}^{-1}$, $\gamma = 1 \text{ ns}^{-1}$, $\kappa = 125 \text{ ns}^{-1}$, $\alpha = 3$, $\eta = 1.2$, $\gamma_a = 0.1 \text{ ns}^{-1}$, $\gamma_p = 0.1 \text{ ns}^{-1}$, with (a) $\theta = 0^\circ$ (b) $\theta = 20^\circ$. Solid lines: results from equation (17). Circles: numerical results for out-of-phase solution. Asterisks: numerical results for in-phase solution.

that the laser will exhibit single-polarisation output. When one solution becomes unstable and the other is stable, PS will occur [41]. In regions where both solutions are unstable, oscillatory behaviour is found [17]. More complicated dynamics, including hysteresis behaviour and period-doubling or quasiperiodic routes to chaos, are also predicted for specific pumping conditions [42].

Finally, the result of equation (19) has been used to estimate the dependence of the maximum ‘spin amplification’ (rate of change of output ellipticity with pump ellipticity) on the SFM parameters in a companion paper [43].

4. Discussion

A common problem in modelling spin-VCSEL behaviour is the difficulty of determining numerical values for the parameters used in the SFM equations. Whilst values of parameters such as the carrier recombination rate γ , photon field decay rate κ and linewidth enhancement factor α are likely to be similar to those in conventional VCSELs, the values of the SFM-specific parameters of birefringence rate γ_p , dichroism rate γ_a and spin relaxation rate γ_s are much less well-known. These latter parameters are difficult to calculate theoretically with any degree of confidence although recent progress in the

understanding of strain-induced birefringence [15, 16] and spin dynamics [44, 45] is relevant here. Also, whilst experimental techniques for the measurement of these parameters in conventional VCSELs have been demonstrated [46–50], these have not yet been applied to spin-VCSELs. Hence it is frequently necessary to estimate parameter values by fitting to measured data on device characteristics such as light-pumping curves, polarisation responses and transient behaviour. In this respect it is anticipated that the expressions derived here will be of assistance in determining parameter values from measured polarisation responses of spin-VCSELs. The advantage of algebraic expressions over numerical simulation here is that trends with parameters can be identified much more rapidly.

5. Conclusion

It has been demonstrated that by assuming that the carrier recombination time is much greater than both the spin relaxation time and the photon lifetime, the steady-state SFM equations for a spin-VCSEL can be solved to yield a closed-form expression between the normalised pumping rate η , the ellipticity of the pump P and the ellipticity of the VCSEL output ε . In-phase and out-of-phase solutions are determined by choice of the sign before a square root. The effect of misalignment between the principal axes of birefringence and dichroism is included; when the misalignment is zero, a rather simpler algebraic expression is found. For small values of VCSEL output ellipticity this expression simplifies still further to give the rate of change of output ellipticity with pump ellipticity which is a measure of the amplification of spin information [8, 43].

Tests of the derived algebraic expressions against numerical solutions of the steady-state SFM equations show that a high degree of accuracy is achieved by this approximation; plotted results are indistinguishable by eye. A ‘Z’-shaped response can occur for the in-phase solutions and the conditions for this to occur are accurately predicted by the approximation in terms of a critical pump rate for given combinations of SFM parameters. Crossing points of the in-phase and out-of-phase solutions is another test where analytic expressions for the co-ordinates are in excellent agreement with numerical simulations.

Acknowledgments

This paper is dedicated to the memory of our former colleague Naci Balkan. The work was supported by the Engineering and Physical Sciences Research Council (Grant No. EP/M024237/1).

ORCID iDs

Mike Adams  <https://orcid.org/0000-0001-9098-6528>

References

- [1] Žutić I, Fabian J and Das Sarma S 2004 *Rev. Mod. Phys.* **76** 323–410
- [2] Gerhardt N C and Hofmann M R 2012 *Adv. Opt. Technol.* **2012** 268949
- [3] Rudolph J, Hagele D, Gibbs H M, Khitrova G and Oestreich M 2003 *Appl. Phys. Lett.* **82** 4516–8
- [4] Rudolph J, Dohrmann S, Hagele D, Oestreich M and Stolz W 2005 *Appl. Phys. Lett.* **87** 241117
- [5] Holub M, Shin J, Saha D and Bhattacharya P 2007 *Phys. Rev. Lett.* **98** 146603
- [6] Vurgaftman I, Holub M, Jonker B and Meyer J 2008 *Appl. Phys. Lett.* **93** 31102
- [7] Hövel S, Gerhardt N, Hofmann M, Yang J, Reuter D and Wieck A 2005 *Electron. Lett.* **41** 251–3
- [8] Gerhardt N, Hövel S, Hofmann M, Yang J, Reuter D and Wieck A 2006 *Electron. Lett.* **42** 88–9
- [9] Hövel S, Bischoff A, Gerhardt N C, Hofmann M R, Ackemann T, Kroner A and Michalzick R 2008 *Appl. Phys. Lett.* **92** 041118
- [10] Schires K, Al Seyab R, Hurtado A, Korpiljärvi V-M, Guina M, Henning I D and Adams M J 2012 *Opt. Express* **20** 3550–5
- [11] Alharthi S S, Al Seyab R, Henning I D and Adams M J 2014 *IET Optoelectron.* **8** 117–21
- [12] Li M, Jähme H, Soldat H, Gerhardt N, Hofmann M and Ackemann T 2010 *Appl. Phys. Lett.* **97** 191114
- [13] Gerhardt N, Li M, Jähme H, Höpfner H, Ackemann T and Hofmann M 2011 *Appl. Phys. Lett.* **99** 151107
- [14] Höpfner H, Lindemann M, Gerhardt N C and Hofmann M R 2014 *Appl. Phys. Lett.* **104** 022409
- [15] Faria P E, Xu G, Lee J, Gerhardt N C, Sipahi G M and Žutić I 2015 *Phys. Rev. B* **92** 075311
- [16] Lindemann M, Pusch T, Michalzick R, Gerhardt N C and Hofmann M R 2016 *Appl. Phys. Lett.* **108** 042404
- [17] Torre M S, Susanto H, Li N, Schires K, Salvide M F, Henning I D, Adams M J and Hurtado A 2017 *Opt. Lett.* **42** 1628–31
- [18] Gøthgen C, Oszwaldowski R, Petrou A and Žutić I 2008 *Appl. Phys. Lett.* **93** 042513
- [19] Saha D, Basu D and Bhattacharya P 2010 *Phys. Rev. B* **82** 205309
- [20] Lee J, Falls W, Oszwaldowski R and Žutić I 2010 *Appl. Phys. Lett.* **97** 041116
- [21] Bhattacharya P, Basu D, Das A and Saha D 2011 *Semicond. Sci. Technol.* **26** 014002
- [22] Holub M and Bhattacharya P K 2007 *J. Phys. D: Appl. Phys.* **40** R179–203
- [23] Basu D, Saha D and Bhattacharya P 2009 *Phys. Rev. Lett.* **102** 093904
- Basu D, Saha D and Bhattacharya P 2009 *Phys. Rev. Lett.* **102** 129901 (erratum)
- [24] Oszwaldowski R, Gøthgen C and Žutić I 2010 *Phys. Rev. B* **82** 085316
- [25] San Miguel M, Feng Q and Moloney J V 1995 *Phys. Rev. A* **52** 1728–39
- [26] Martin-Regalado J, Pratl F, San Miguel M and Abraham N B 1997 *IEEE J. Quantum Electron.* **33** 765–83
- [27] Gahl A, Balle S and San Miguel M 1999 *IEEE J. Quantum Electron.* **33** 342–51
- [28] Travagnin M, van Exter M P, Jansen van Doorn A K and Woerdman J P 1997 *Phys. Rev. A* **54** 1647–60
- Travagnin M, van Exter M P, Jansen van Doorn A K and Woerdman J P 1997 *Phys. Rev. A* **55** 4641 (erratum)
- [29] Dyson A and Adams M J 2003 *J. Opt. B: Quantum Semiclass. Opt.* **5** 222–6
- [30] Gerhardt N, Hövel S, Hofmann M, Yang J, Reuter D and Wieck A 2006 *Electron. Lett.* **42** 88–9

- [31] Adams M J and Alexandropoulos D 2009 *IEEE J. Quantum Electron.* **45** 744–9
- [32] Balle S, Tolkachova E, San Miguel M, Tredicce J R, Martín-Regalado J and Gahl A 1999 *Opt. Lett.* **24** 1121–3
- [33] Travagnin M 1997 *Phys. Rev. A* **56** 4094–105
- [34] Mulet J and Balle S 2002 *IEEE J. Quantum Electron.* **38** 291–305
- [35] Masoller C and Torre M S 2008 *Opt. Express* **16** 21282–96
- [36] Adams M J and Alexandropoulos D 2012 *IEEE Photonics J.* **4** 1124–32
- [37] Qasaimeh O 2015 *Opt. Quantum Electron.* **47** 465–76
- [38] Erneux T, Danckaert J, Panajotov K and Veretennicoff I 1999 *Phys. Rev. A* **59** 4660–7
- [39] Virte M, Sciamanna M, Mercier E and Panajotov K 2014 *Opt. Express* **22** 6772–7
- [40] Virte M, Mirisola E, Sciamanna M and Panajotov K 2015 *Opt. Lett.* **40** 1865–8
- [41] Susanto H, Schires K, Adams M J and Henning I D 2015 *Phys. Rev. A* **92** 063838
- [42] Li N, Susanto H, Cemlyn B R, Henning I D and Adams M J 2017 *Phys. Rev. A* **96** 013840
- [43] Cemlyn B R, Adams M, Harbord E, Li N, Henning I, Oulton R, Korpijärvi V-M and Guina M 2018 *Semicond. Sci. Technol.* submitted
- [44] Szolnoki L, Dóra B, Kiss A, Fabian J and Simon F 2017 *Phys. Rev. B* **96** 245123
- [45] Vaughan M P and Rorison J M 2018 *Semicond. Sci. Technol.* **33** 014001
- [46] van Exter M P, Willemsen M B and Woerdman J P 1998 *Phys. Rev. A* **58** 4191–205
- [47] Pérez P, Valle A and Pesquera L 2014 *J. Opt. Soc. Am. B* **31** 2574–80
- [48] Quirce A, Valle A, Pesquera L, Thienpont H and Panajotov K 2015 *J. Sel. Top. Quantum Electron.* **21** 1800207
- [49] Frougier J, Baili G, Sagnes I, Dolfi D, George J-M and Alouini M 2015 *Opt. Express* **23** 9573–88
- [50] Yang J Y, Wu Z M, Liang Q, Chen J J, Zhong Z Q and Xia G Q 2016 *Acta Phys. Sin.* **65** 124203